Numerical analysis of advection-diffusion problems on 2D general-shaped domains by means of a RBF Collocation Meshless Method

IOP Conf. Series: Journal of Physics: Conf. Series **1224** (2019) 012013 doi:10.1088/1742-6596/1224/1/012013

Numerical analysis of advection-diffusion problems on 2D general-shaped domains by means of a RBF Collocation Meshless Method

Riccardo Zamolo[1] **and Enrico Nobile**[1]

[1] Dipartimento di Ingegneria e Architettura, Università degli Studi di Trieste, via A. Valerio 10, 34127 Trieste, Italy

E-mail: riccardo.zamolo@phd.units.it

Abstract. A Collocation Meshless Method based on local Radial Basis Function (RBF) interpolation is employed to solve two-dimensional advection-diffusion problems with particular reference to the incompressible Navier-Stokes equations in their transient form, i.e., unsteady flows, using primitive variables $(\mathbf{u}, p)$. A projection scheme is employed to decouple the continuity and momentum equations; particular attention is given to the choice of the required solvers. This approach is applied to the simulation of unsteady flows for two typical test cases, i.e., the lid-driven cavity problem and the flow past a circular cylinder between parallel walls. Numerical results compare very favorably with literature ones, confirming that this approach can be effectively employed in the numerical simulation of unsteady flows on practical geometries where complex node distributions and large number of nodes are required.

Keywords:
Navier-Stokes equations, Poisson equation, multigrid, node distribution, fluid flow

1. Introduction

The simulation of engineering problems with widely used numerical approaches such as Finite Element and Finite Volume methods requires a spatial discretization of the domain; this meshing phase can require a significant effort, especially when dealing with complex geometries of practical relevance where the mesh must fulfill particular properties.

In order to avoid the need of a classic mesh, in recent years several meshless approaches have been proposed [1]: the mesh is replaced by a simple distribution of nodes which easily adapts to complex geometries; then some formal interpolation on this set of nodes is required in order to approximate differential quantities from nodal values. Being this a very generic approach, it can be applied to a wide range of problems including heat transfer [2, 3], solid mechanics and fluid flow [4].

Meshless methods employing local Radial Basis Function (RBF) interpolation [5–8], also known as RBF generated Finite Differences methods (RBF-FD), are particularly attractive for practical fluid flow problems because of their geometrical flexibility and computational efficiency due to the local formulation, and will be used in this paper for such purpose; furthermore, the local formulation allows the use of very efficient solvers.

The numerical approach presented here will be applied to the simulation of two-dimensional unsteady flows for two well-known test cases: the lid-driven cavity at $Re = 1000$ and $Re = 5000$, and the flow past a circular cylinder between parallel walls at Re ranging from 100 to 1000. Very good agreement to literature results is found for each of these test cases, showing that the proposed approach can be an accurate and efficient tool in the numerical simulation of unsteady fluid flow problems over geometries of practical relevance.

2. Governing equations and boundary conditions

Let us consider an incompressible fluid with density ρ and constant kinematic viscosity ν. The resulting two-dimensional Navier-Stokes equations can be made dimensionless by taking H, u_0, H/u_0 and ρu_0^2 as reference quantities for length, velocity, time and pressure, respectively, obtaining the following nondimensional momentum and continuity equations:

$$\frac{\partial \mathbf{u}}{\partial t} + (\mathbf{u} \cdot \nabla)\mathbf{u} = -\nabla p + \frac{1}{Re}\nabla^2 \mathbf{u} \tag{1}$$

$$\nabla \cdot \mathbf{u} = 0 \tag{2}$$

where $Re = u_0 H/\nu$ is the flow Reynolds number. No-slip conditions, i.e., $\mathbf{u} = \mathbf{u}_W$, are imposed at all solid walls with velocity $\mathbf{u}_W$; in the case of the flow past a circular cylinder, velocity is imposed at the inlet while fully developed flow conditions, i.e., $\partial \mathbf{u}/\partial \mathbf{n} = \mathbf{0}$ with $\mathbf{n}$ the outward unit normal, are imposed at the outlet.

3. Numerical method

3.1. 2D node distributions

The two-dimensional node distributions, i.e., a set of N nodes $\mathbf{x}_i$, required by the RBF-FD meshless discretizations have been obtained through the modified Quadtree algorithm followed by repel refinement proposed in [9]; such algorithm is briefly summarized here.

Given a prescribed spacing function $s(\mathbf{x})$ which defines the local spacing between the nodes, an initial node distribution is obtained through the Quadtree algorithm modified with a dithering correction in order to reduce the nodal quantization error, i.e., the difference between the integer number of nodes that can be contained in any set Ω and the prescribed (non-integer) number $\int_\Omega s(\mathbf{x})^{-2}\ \mathrm{d}\omega$. The resulting node distribution is then improved by the application of 50 refinement iterations based on radial repel forces between the nodes.

3.2. Local RBF interpolation

RBF interpolation approximates the generic field ξ around $\mathbf{x}$ through the following expansion:

$$\xi(\mathbf{x}) = \sum_{j \in J_q(\mathbf{x})} a_j \varphi(\|\mathbf{x} - \mathbf{x}_j\|) + \mathbf{b}^T \mathbf{x} + c \tag{3}$$

where $J_q(\mathbf{x})$ is the set of the indices j of the q nodes $\mathbf{x}_j$ closest to $\mathbf{x} = (x, y)^T$. $\xi(\mathbf{x})$ is a linear combination of q radial functions φ centered at the q nodes $\mathbf{x}_j$ plus a linear polynomial in $\mathbf{x}$. In this work $q = 7$ local nodes have been chosen because the employed multicloud solver [10] is specifically developed and optimized for this choice. Hardy's Multiquadric has been chosen as radial function since it seems to offer the better results if an appropriate shape factor ε is employed [11]:

$$\varphi(r) = \sqrt{1 + (\varepsilon r)^2} \tag{4}$$

where the shape factor has been rescaled as $\varepsilon = \bar{\varepsilon} s_M / d_n(\mathbf{x})$ with s_M the maximum spacing function over the domain and $d_q(\mathbf{x})$ the local subdomain size [3]. In this work we employed $\bar{\varepsilon} = 1$ since it is a reasonable trade-off between accuracy and numerical stability [12].

The coefficients a_j, $\mathbf{b}$ and c can be formally computed imposing the canonical interpolation conditions for the $m \leq q$ local nodes $\mathbf{x}_i$, $i \in J_q(\mathbf{x})$ which do not lie on the portion of the boundary where Neumann conditions are imposed on ξ:

$$\xi(\mathbf{x}_i) = \xi_i \tag{5}$$

where ξ_i is the nodal value of ξ in $\mathbf{x}_i$.

The following additional relations are needed in order to ensure linear reproducibility of Equation (3):

$$\sum_{j \in J_q(\mathbf{x})} a_j = 0 \quad , \quad \sum_{j \in J_q(\mathbf{x})} x_j a_j = 0 \quad , \quad \sum_{j \in J_q(\mathbf{x})} y_j a_j = 0 \tag{6}$$

If any of the local nodes $\mathbf{x}_i$, $i \in J_q(\mathbf{x})$ lies on the Neumann boundary, for each of these $q - m$ Neumann nodes the corresponding boundary condition must be satisfied:

$$\frac{\partial \xi}{\partial \mathbf{n}}\Big|_{\mathbf{x}=\mathbf{x}_i} = 0 \tag{7}$$

where the normal derivative of ξ is obtained from Equation (3), and only homogeneous Neumann boundary conditions are required in the presented problems.

Collecting the n coefficients a_i and the m unknown values ξ_i in column vectors $\mathbf{a}$ and $\boldsymbol{\xi}$, respectively, the interpolation system is the following:

$$\mathbf{G} \begin{Bmatrix} \mathbf{a} \\ \mathbf{b} \\ c \end{Bmatrix} = \begin{Bmatrix} \boldsymbol{\xi} \\ \mathbf{0} \end{Bmatrix} \tag{8}$$

3.3. Collocation

A generic linear partial differential equation $L(\xi) = b$ with the local RBF approximation expressed by Equation (3) becomes:

$$\sum_{j \in J_n(\mathbf{x})} a_j L\big(\varphi(\|\mathbf{x} - \mathbf{x}_j\|)\big) + \mathbf{b}^T L(\mathbf{x}) + cL(1) = b(\mathbf{x}) \tag{9}$$

Writing the previous equation in compact form for a generic node $\mathbf{x}_k$ near $\mathbf{x}$ gives:

$$L\big(\{\boldsymbol{\varphi}^T \ \mathbf{x}^T \ 1\}\big)|_{\mathbf{x}=\mathbf{x}_k} \begin{Bmatrix} \mathbf{a} \\ \mathbf{b} \\ c \end{Bmatrix} = b(\mathbf{x}_k) \tag{10}$$

where $\boldsymbol{\varphi}$ is the column vector of the q local RBF φ and L acts element-wise on vectors. Finally, recalling $\mathbf{a}$, $\mathbf{b}$ and c from Equation (8) we obtain:

$$L\big(\{\boldsymbol{\varphi}^T \ \mathbf{x}^T \ 1\}\big)|_{\mathbf{x}=\mathbf{x}_k} \mathbf{G}^{-1} \begin{Bmatrix} \boldsymbol{\xi} \\ \mathbf{0} \end{Bmatrix} = b(\mathbf{x}_k) \tag{11}$$

Writing Equation (11) for each internal node $\mathbf{x}_k$, i.e., which does not lie on the boundary, gives the final linear system:

$$\mathbf{A}_{II} \boldsymbol{\xi}_I = \mathbf{b} - \mathbf{A}_{ID} \boldsymbol{\xi}_D \tag{12}$$

where the subscripts I and D refer to *Internal* and *Dirichlet* contributions, respectively; $\mathbf{A}_{II}$ is sparse and non-symmetric.

The presented RBF-FD discretization approach is proven to be second order accurate in space for second order elliptic problems [9, 10].

3.4. Solution procedure

At each time step, the computation of velocity and pressure through Equations (1) and (2) is decoupled using a traditional projection scheme with a three-level Gear scheme for the time discretization; first, a tentative velocity $\mathbf{u}^*$ is computed from the linearized momentum equation:

$$\frac{3\mathbf{u}^* - 4\mathbf{u}^n + \mathbf{u}^{n-1}}{2\Delta t} + \tilde{\mathbf{u}}^{n+1}\nabla\mathbf{u}^* = -\nabla p^n + \frac{1}{Re}\nabla^2\mathbf{u}^* \tag{13}$$

where $\tilde{\mathbf{u}}^{n+1} = 2\mathbf{u}^n - \mathbf{u}^{n-1}$ is the extrapolated velocity at timestep $n+1$ and Δt is the time step size. Then, the computed tentative velocity $\mathbf{u}^*$ is forced to satisfy the continuity equation (2) by means of an irrotational correction $\mathbf{u}^{n+1} = \mathbf{u}^* - \nabla\phi$ (Helmholtz-Hodge decomposition) resulting in a Poisson equation in the auxiliary variable ϕ with homogeneous Neumann boundary conditions:

$$\nabla^2\phi = \nabla\cdot\mathbf{u}^* \tag{14}$$

The pressure is then updated as $p^{n+1} = p^n + \phi/\Delta t$.

Equations (13) and (14) are discretized using the previously presented local RBF collocation technique, resulting in a scheme with second order accuracy in both time and space. The momentum equation (13), consisting in 2 scalar equations for $\mathbf{u} = (u, v)^T$, is solved using the BiCGSTAB [13] iterative method with an additive correction multicloud (ACMC) technique as preconditioner [10], using 10^{-9} as target normalized RMS norm for the residuals; such choice for the momentum equations solver is motivated by the fact that the coefficient matrices for these equations change at each time since the advective term is treated implicitly, therefore a fast and iterative solver must be used. For the present test cases, the following ACMC parameters have been used: SOR iteration multiplier $r_I = 2$, SOR relaxation factor $\omega \in [0.7, 1.3]$ and overcorrection factor $t_{oc} \in [0.7, 1.8]$; the smallest values for ω and t_{oc} have been employed for the high Re cases in order to ensure the convergence of each scalar equation in less than 180-200 Work Units (1 WU = 1 residual evaluation at the fine level).

The Poisson equation (14) is solved through a LU decomposition of the corresponding coefficient matrix since it is constant and therefore the factorization can be performed once at the beginning of the simulation and the Poisson solution phase at each time step is very fast; nonetheless, this approach is not efficient with large number of nodes, e.g., $N > 2.5 \div 5 \cdot 10^5$, because of the excessive growth of memory and time requirements of the LU approach. In such cases an iterative approach similar to the one used for momentum equations must be employed.

The computational costs are comparable to the ones obtained with a FEM discretization with linear triangular elements on isotropic meshes where the stencil size for each node is comparable to the present choice $q = 7$.

In the case of the extension of the method to practical 3D problems, the following techniques can be employed for the efficient solution of the systems of equations arising from the RBF-FD discretization of both Poisson and momentum equations:

- BiCGSTAB method with incomplete LU factorization (ILU) [14];
- algebraic multigrid (AMG) [15];
- a 3D extension of the multicloud techniques presented in [10].

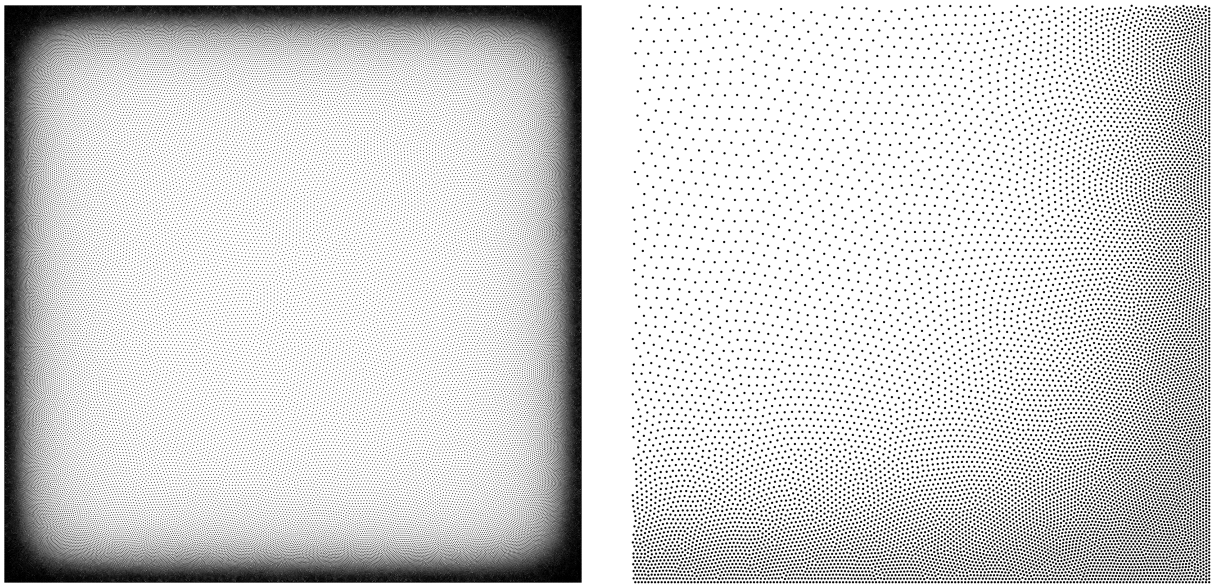

Figure 1. Node distribution for the lid-driven cavity problem with $N \approx 10^5$ nodes (left) and enlarged view of the bottom right corner (right).

3.5. Auxiliary computations

The streamfunction ψ is calculated solving the Poisson equation $\nabla^2\psi = -\nabla \times \mathbf{u}$ using the same node distributions and the same local RBF collocation technique employed for the discretization of the momentum and Poisson equations of the problem itself. Dirichlet boundary conditions are employed: $\psi = 0$ at all solid walls in the case of the lid-driven cavity problem, $\psi = \bar{\psi}$ in the case of the flow past a circular cylinder, where $\bar{\psi}$ is coherent with velocity boundary conditions, i.e., $\bar{\psi} = const$ along solid walls and $\partial\bar{\psi}/\partial y = u$ along the vertical inlet and outlet.

3.6. Implementation details

The presented procedures has been implemented in MATLAB® environment using MATLAB linked MEX functions which are compiled from C source code for the computational expensive tasks, on a modern laptop Intel® i7 2.6GHz with 4 cores and 8 threads. Multi-core parallelism is achieved using OpenMP® API for the C source code employed in the coefficients calculations and multicloud operations, i.e., SOR smoothing iterations, residual evaluation and restriction. Some of the remaining MATLAB operations, including BiCGSTAB algorithm, are natively parallelized on all available cores in MATLAB by default. The typical computing time is 0.9 s/time step with $N \approx 10^5$ nodes for each Re and Δt employed in this work.

4. Numerical results and discussion

4.1. Lid-driven cavity problem

The domain of the problem is the square cavity $[0, H]^2$ where the top wall moves with velocity $\mathbf{u}_W = (u_0, 0)^T$.

The spacing function $s(\mathbf{x})$ is defined as follows:

$$\frac{5s}{s_M} = 1 + \Big[1 + \cos\big(\pi(2\bar{x} - 1)\big)\Big]\Big[1 + \cos\big(\pi(2\bar{y} - 1)\big)\Big] \tag{15}$$

where $\bar{x} = x/H$ and $\bar{y} = y/H$ are the nondimensional coordinates. A node distribution with $N \approx 10^5$ nodes is depicted in Figure 1 together with an enlarged view of one corner; as it can

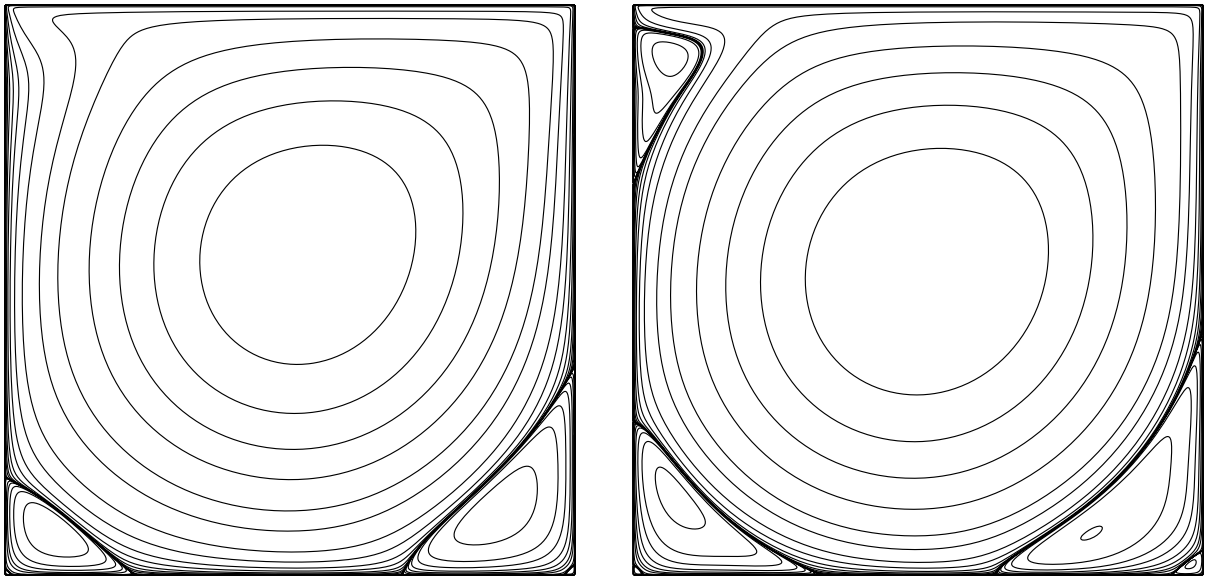

Figure 2. Streamfunction contours for the lid-driven cavity problem at $Re = 1000$ (left) and $Re = 5000$ (right).

Table 1. Streamfunction values for streamline plots.

-1×10^{-1}	-8×10^{-2}	-6×10^{-2}	-4×10^{-2}	-2×10^{-2}	-1×10^{-2}	-3×10^{-3}	-1×10^{-3}
-3×10^{-4}	-1×10^{-4}	-3×10^{-5}	-1×10^{-5}	-3×10^{-6}	-1×10^{-6}	-1×10^{-7}	-1×10^{-8}
-1×10^{-9}	-1×10^{-10}	-1×10^{-11}	-1×10^{-12}	-1×10^{-13}	-1×10^{-14}	0	1×10^{-14}
1×10^{-13}	1×10^{-12}	1×10^{-11}	1×10^{-10}	1×10^{-9}	1×10^{-8}	1×10^{-7}	1×10^{-6}
3×10^{-6}	1×10^{-5}	3×10^{-5}	1×10^{-4}	3×10^{-4}	1×10^{-3}	3×10^{-3}	1×10^{-2}

be seen, the previously defined spacing function decreases from the center of the cavity, where $s = s_M$, towards the walls, where $s = s_M/5$, in order to better resolve the boundary layers.

Starting from rest, a steady state solution for $Re = 1000$ is obtained after about 200 time units with $\Delta t = 0.05$ and $N \approx 10^5$ nodes. The case $Re = 5000$ is started from the steady state solution at $Re = 1000$ and a steady state solution is again found after about 200 time units with $\Delta t = 0.025$. The streamfunction contours for the values reported in Table 1 are depicted in Figure 2 for both $Re = 1000$ and $Re = 5000$ and show very good agreement, to graphical accuracy, with the results reported in [5, 16].

The values of the extrema of streamfunction and the corresponding locations for primary and secondary vortexes are reported in Table 2 where the results from other authors are also reported for comparison: these results show very good agreement with reference values in both cases $Re = 1000$ and $Re = 5000$, with less than 1% deviations for both strengths and locations of the streamfunction extrema in each case.

4.2. Flow past a circular cylinder between parallel walls

Table 2. Comparison of streamfunction extrema for $Re = 1000$ and $Re = 5000$.

	Primary vortex, ψ (location)	Secondary vortex BR, ψ (location)	Secondary vortex BL, ψ (location)
		$Re = 1000$	
Bayona [5]	-0.1189 (0.5308,0.5652)	1.730E-3 (0.8641,0.1118)	2.334E-4 (0.0832,0.0781)
Nobile [16]	-0.1175 (0.5313,0.5625)	1.770E-3 (0.8594,0.1094)	2.320E-4 (0.0859,0.0781)
Present res.	-0.1188 (0.5327,0.5674)	1.726E-3 (0.8623,0.1111)	2.321E-4 (0.0840,0.0781)
		$Re = 5000$	
Bayona [5]	-0.1223 (0.5151,0.5352)	3.077E-3 (0.8046,0.0727)	1.379E-3 (0.0728,0.1371)
Nobile [16]	-0.1214 (0.5156,0.5357)	3.096E-3 (0.8058,0.0737)	1.370E-3 (0.0714,0.1384)
Present res.	-0.1227 (0.5141,0.5362)	3.068E-3 (0.8032,0.0715)	1.366E-3 (0.0734,0.1380)

BR = bottom right; BL = bottom left.

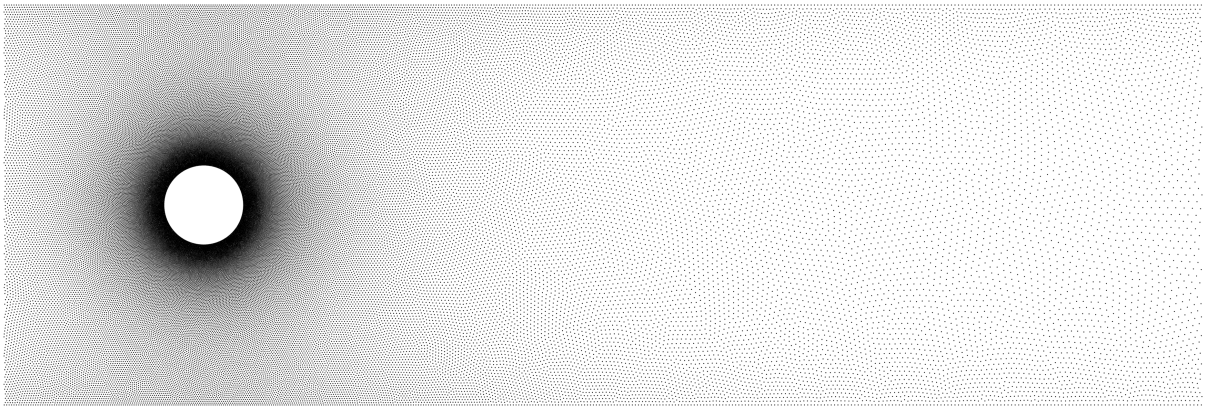

Figure 3. Particular of the node distribution near the circular cylinder ($-0.5H < x < 2.5H$) with $N \approx 10^5$ nodes.

Table 3. Comparison of nondimensional period T and time-averaged drag coefficient C_D.

	Re	100	200	240	300	500	750	1000
Present	T	–	–	0.85	0.80	0.73	0.69	0.66
results	C_D	4.65	3.37	3.15	2.98	2.76	2.75	2.75
Zovatto and	T	–	–	0.85	0.81	0.73		0.67
Pedrizzetti [17]	C_D	4.68	3.40	3.19	2.97	2.71	2.68	2.64

The domain of the problem is a plane channel with width $11H$ and height H between the horizontal walls, containing a circular cylinder with diameter $d = 0.2H$ centered at the half of the channel height and $3H$ from the vertical left inlet; therefore the vertical right outlet is positioned $8H$ to the right of the cylinder center, which is also the origin of the coordinate system. A Poiseuille velocity profile $u = 6u_0[1/4 - (y/H)^2]$, which has an average velocity u_0, is imposed at the inlet, while fully developed flow conditions $\partial \mathbf{u}/\partial x = \mathbf{0}$ are imposed at the outlet; although a real fully developed flow is not obtained at the end of the channel, especially for high

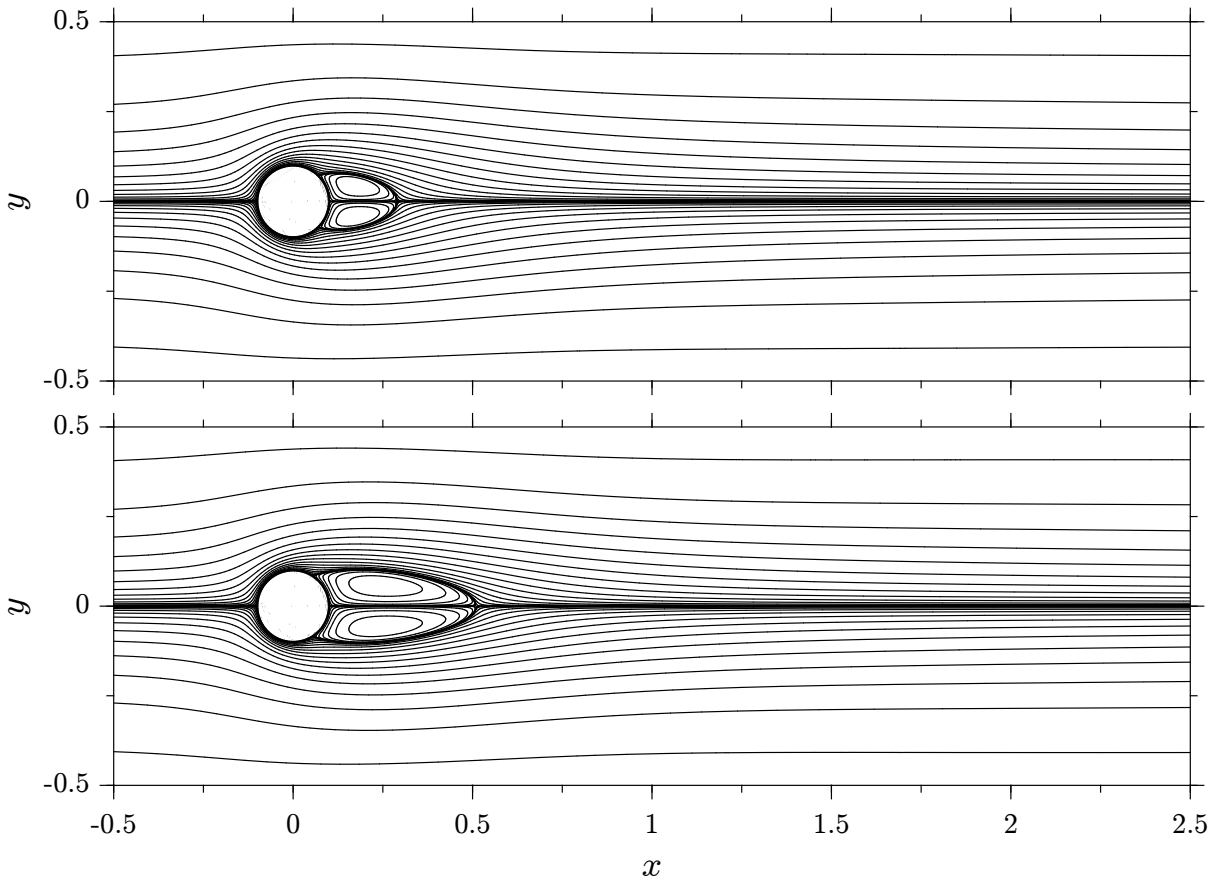

Figure 4. Streamlines for the steady flow past a circular cylinder with $Re = 100$ (top) and $Re = 200$ (bottom).

Re, the channel extension downstream of the cylinder, i.e., $8H = 40d$, is enough to avoid any appreciable influence of the outlet boundary conditions on the flow near the cylinder.

The spacing function is defined as follows:

$$\frac{s_M}{s} = 1 + k_W \left(\frac{2y}{H}\right)^{2e_W} + k_C \frac{d}{2r} \tag{16}$$

where $k_W = 3$, $e_W = 1.75$, $k_C = 24$ and r is the distance from the center of the cylinder; therefore the ratio between the nodal spacing at the horizontal walls and the maximum spacing is approximately $1/(k_W + 1) = 1/4$, while the ratio between the nodal spacing at the cylinder wall and the maximum spacing is approximately $1/(k_C + 1) = 1/25$. An enlarged view of the node distribution near the cylinder for $N \approx 10^5$ nodes is depicted in Figure 3 where it can be seen that the nodal density near the cylinder is very high in order to better resolve the boundary layers.

Simulations are carried out with the same node distribution with $N \approx 10^5$ nodes for $Re = 100$, 200, 240, 300, 500, 750 and 1000; each case is started with the last available solution at Re immediately below, except for the case $Re = 100$ which is started from rest.

Steady state solutions are obtained after about 20 time units for $Re = 100$ and $Re = 200$ with $\Delta t = 0.025$. The boundary conditions for streamfunction are set to obtain $\psi(x, 0) = 0$ at the half of the channel height; the streamfunction contours for these steady solutions are depicted in Figure 4 for values of ψ ranging from $\psi(x, -H/2)$ (streamfunction at bottom wall)

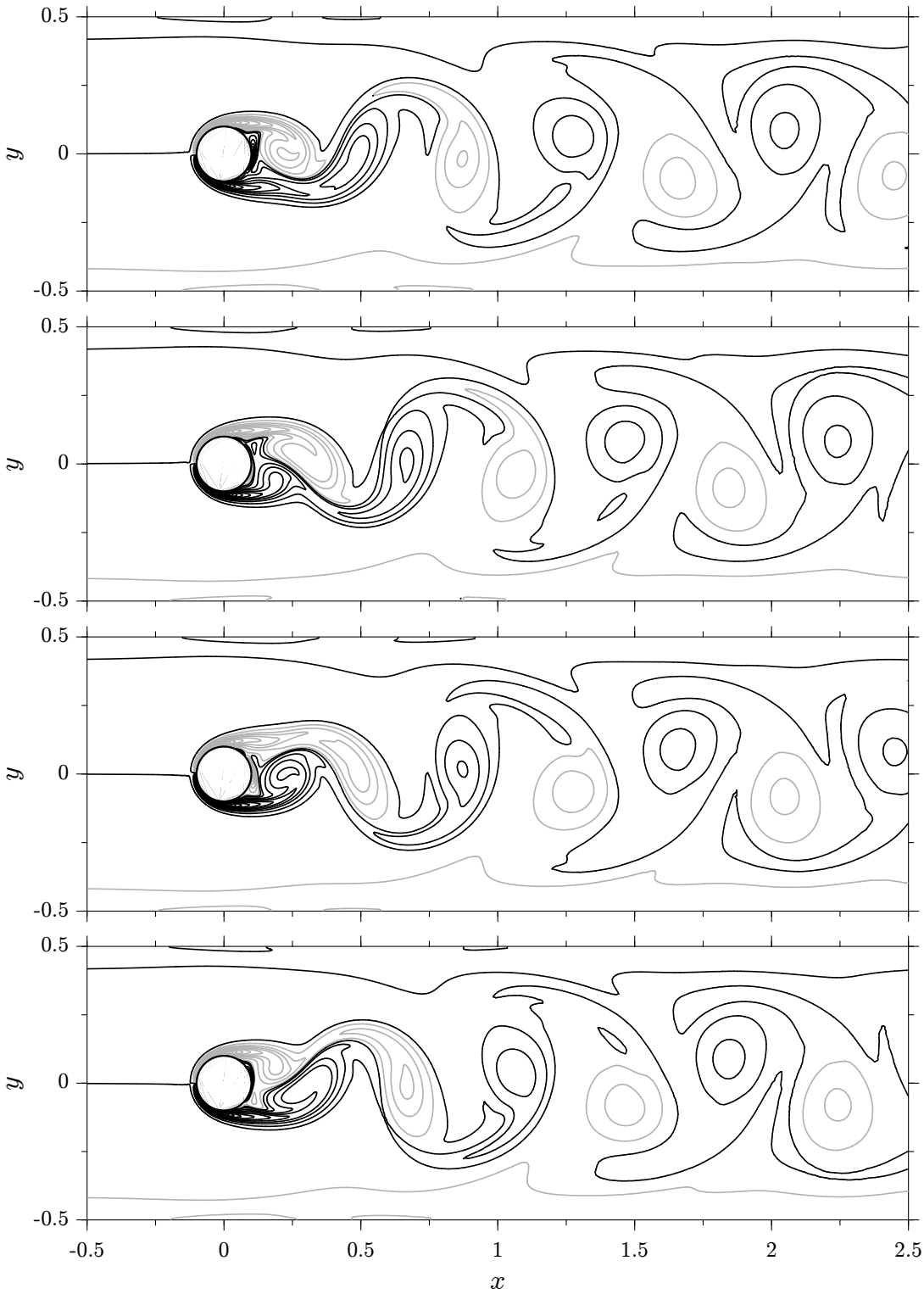

Figure 5. Vorticity contours for $Re = 1000$ at 4 equally spaced times over a period T.

to $\psi(x, H/2)$ (streamfunction at top wall) as the power ψ^5 in order to highlight the streamlines in the wakes. Very good agreement is found, to graphical accuracy, with the results reported in

[18].

The solution for $Re = 240$, as expected, is not stable and a periodical solution is found after about 90 time units with $\Delta t = 0.025$; this is in perfect accordance with the results of [19] which show that the critical Re is 231. Periodical solutions with period T are found for each of the higher Re considered, with periodical vortex shedding behind the cylinder. For $Re = 750$ and $Re = 1000$ the time step has been reduced from $\Delta t = 0.025$ to $\Delta t = 0.02$ in order to allow the convergence of momentum equations in less than 200 Work Units, at the price of more time steps per period T. Contour plots for vorticity in the case $Re = 1000$ are depicted in Figure 5 for vorticity values starting from ± 5 and increasing with constant steps ± 10; again, very good agreement is found, to graphical accuracy, with the results reported in [17].

A comparison with literature results is reported in Table 3 for the period T and the drag coefficient $C_D = 2F_x/\rho u_0^2 H d$, where F_x is the x-component of the force exerted by the fluid on the cylinder, which is time-averaged over a period T in the case of periodical flows. Numerical results compare very favorably with reference values for each of the considered Re, with less than 5% deviations for C_D and less than 2% deviations for T.

5. Conclusions

In this work a collocation meshless approach, based on local RBF interpolation, is used for the numerical simulation of unsteady fluid flow problems using primitive variables, i.e., velocity and pressure, on 2D domains with complex node distributions of practical relevance. A projection scheme is employed to decouple the momentum and continuity equation; particular attention is given to the choice of the solvers in order to obtain an efficient solution procedure. The lid-driven cavity problem and the flow past a circular cylinder have been chosen as test cases to highlight the properties of the presented numerical scheme; several computations for different Reynolds numbers are carried out in order to validate the proposed meshless approach at different flow regimes.

Numerical results for these test problems agree very favorably with previous numerical studies for each of the considered cases; along with the computational efficiency, such results suggest that the proposed meshless approach can be extremely effective in the numerical simulation of unsteady fluid flow problems on general-shaped 2D domains with node distributions of practical engineering relevance; this approach can also be extended to 3D problems with remarkable geometrical advantages over standard mesh-based methods.

References

[1] Li H and Mulay S 2013 *Meshless Methods and Their Numerical Properties* (CRC Press) ISBN 978-1-4665-1747-9
[2] Šarler B and Vertnik R 2006 *COMPUT MATH APPL* **51**(8) 1269–1282
[3] Mavric B and Šarler B 2015 *INT J NUMER METHOD H* **25**(6) 1488–1510
[4] Kosec G and Šarler B 2008 *INT J NUMER METHOD H* **18**(7/8) 868–882
[5] Bayona V, Flyer N, Fornberg B and Barnett G 2017 *J COMPUT PHYS* **332** 257 – 273
[6] Fornberg B and Flyer N 2015 *ACTA NUMER* **24** 215–258
[7] Sarra S and Kansa E 2009 *Multiquadric Radial Basis Function Approximation Methods for the Numerical Solution of Partial Differential Equations* (*Advances in Computational Mechanics* vol 2) ed Atluri S N (Tech Science Press)
[8] Waters J and Pepper D 2015 *NUMER HEAT TR B-FUND* **68**(3) 185–203
[9] Zamolo R and Nobile E 2018 *COMPUT MATH APPL* **75**(1)
[10] Zamolo R and Nobile E 2018 *Multicloud techniques for convergence acceleration with local RBF meshless discretizations* (Submitted)
[11] Franke R 1980 A critical comparison of some methods for interpolation of scattered data Tech. rep. NAVAL POSTGRADUATE SCHOOL, Monterey, California
[12] Zamolo R and Nobile E 2017 *J PHYS CONF SER* **923**
[13] van der Vorst H 1992 *SIAM J SCI STAT COMP* **13**(2) 631–644

[14] Saad Y 2003 *Iterative Methods for Sparse Linear Systems* (Philadelphia, Pennsylvania: SIAM) chap 10: Preconditioning Techniques 2nd ed
[15] Stüben K 2001 *J COMPUT ANAL APPL* **128**(1-2) 281–309
[16] Nobile E 1996 *NUMER HEAT TR B-FUND* **30**(3) 351–370
[17] Zovatto L and Pedrizzetti G 2001 *J FLUID MECH* **440** 1–25
[18] Singha S and Sinhamahapatra K 2010 *OCEAN ENG* **37** 757–769
[19] Chen J H, Pritchard W G and Tavener S J 1995 *J FLUID MECH* **284** 23–41